Liquid Crystals
Publication details, including instructions for authors and subscription information:
http://www.informaworld.com/smpp/title~content=t713926090

Twist grain boundary states in non-chiral smectogen-chiral dopant

N. L. Kramarenko; V. I. Kulishov; L. A. Kutulya; G. P. Semenkova; V. P. Seminozhenko; N. I. Shkolnikova

Online publication date: 06 August 2010

To cite this Article Kramarenko, N. L. , Kulishov, V. I. , Kutulya, L. A. , Semenkova, G. P. , Seminozhenko, V. P. and Shkolnikova, N. I.(1997) 'Twist grain boundary states in non-chiral smectogen-chiral dopant', Liquid Crystals, 22: 5, 535 — 541
To link to this Article: DOI: 10.1080/026782997208910
URL: http://dx.doi.org/10.1080/026782997208910

LIQUID CRYSTALS, 1997, VOL. 22, NO. 5, 535–541

Twist grain boundary states in non-chiral smectogen–chiral dopant

by N. L. KRAMARENKO†, V. I. KULISHOV‡, L. A. KUTULYA*†,
G. P. SEMENKOVA†, V. P. SEMINOZHENKO† and N. I. SHKOLNIKOVA†

†Institute for Single Crystals, Academy of Sciences of Ukraine, 60 Lenin Ave, Kharkov 310001, Ukraine

‡Institute of Physics, Academy of Sciences of Ukraine, 46 Pr. Nauki, Kiev 252028, Ukraine

(*Received 17 October 1996; accepted 16 December 1996*)

The liquid crystalline systems studied consisted of non-chiral mesomorphic esters [the eutectic mixture of 4-*n*-hexyloxyphenyl 4-*n*-octyloxybenzoate and 4-*n*-octyloxyphenyl 4-*n*-hexyloxybenzoate] and structurally similar chiral dopants (*N*-arylidene derivatives of *S*-1-phenyl- and *S*-1-benzyl-ethylamine). Twist grain boundary phases occur between the cholesteric and smectic C* or smectic A phases in all the investigated systems. The different structures of these TGB phases (TGB_A and TGB_C) are proved by small angle X-ray scattering and textural studies. The concentration and temperature ranges of the TGB phases are defined by the twisting power of the chiral dopants and their own mesomorphic peculiarities. The experimental dependences of TGB phase temperature range on cholesteric helical twist are influenced by a ratio change of the optically active and racemic forms of the dopant at a constant total concentration. The results obtained are discussed within Renn's theory.

1. Introduction

More than twenty years ago, noticing the formal analogy between superconductors and SmA liquid crystals, de Gennes predicted a liquid crystalline phase similar to the Abrikosov phase in type-II superconductors [1]. In the same way as the magnetic field is expelled from superconductors, the twist distortion is expelled out of the smectic structure in this phase forming a lattice of defect lines. The theoretical model of this new phase structure was proposed in 1988 by Renn and Lubensky [2]: two-dimensional smectic slabs are arrayed along a helix axis parallel to the smectic layers. Adjacent slabs are separated by grain boundaries which consist of a grid of parallel equi-spaced screw dislocation lines to allow for the helical twist. Hence, the name of this phase is twist grain boundary (TGB). The model [2] is extended to tilted smectic phases, distinguishing the TGB_A phase where the molecules are statistically normal to the smectic layers from the TGB_C phase where the molecules are tilted in the smectic layers [3].

The new phase with a local smectic ordering and helical supramolecular structure was first found experimentally by Goodby *et al.* [4] and further assigned to the TGB state [5]. TGB_A and TGB_C phases have been studied by several groups (for example, see [6–8]). However, most research on TGB states has concerned individual liquid crystals that did not give the opportunity to reproduce Renn's phase diagram in full. In our viewpoint, the most favourable materials are liquid crystalline systems with an induced helical supramolecular structure consisting of a non-chiral mesogen and chiral dopant. In such systems, the variation of cholesteric twist can be controlled by the chiral dopant concentration over a wide interval. We have previously presented a phase diagram with a wide TGB phase region for certain binary liquid crystalline systems [9, 10] and then established the influence of the chiral dopant molecular structure on the type of phase diagram and on the TGB regions [11].

In this paper, we present the phase diagrams showing TGB phases for some liquid crystalline systems based on the same non-chiral smectogenic matrix and different chiral dopants. The phenyl benzoate fragment is common to the structurally similar non-chiral mesogens and the chiral dopants used. Such a choice of materials for study allowed us to analyse the data for the influence of chiral dopant molecular structure, their twisting power and their own mesomorphic peculiarities on the types of TGB phases and their overall concentration and temperature ranges. Side by side with a qualitative analysis of the TGB phases, the experimental

*Author for correspondence.

0267–8292/97 $12·00

dependences of the TGB_A and TGB_C temperature ranges on the cholesteric helical twist are presented. The results are discussed on the basis of Renn's theoretical model.

2. Materials

In this work the eutectic composition of 4-*n*-hexyloxyphenyl 4-*n*-octyloxybenzoate and 4-*n*-octyloxyphenyl 4-*n*-hexyloxybenzoate (7:3) (**1**) was used as the non-chiral matrix. This composition has the following temperatures of phase transitions:

$$\text{Cr} \xrightarrow{41^\circ\text{C}} \text{SmC} \xrightarrow{51^\circ\text{C}} \text{N} \xrightarrow{78^\circ\text{C}} \text{I} \xrightarrow{78^\circ\text{C}} \text{N}$$

$$\xrightarrow{51^\circ\text{C}} \text{SmC} \xrightarrow{30^\circ\text{C}} \text{Cr}$$

The chiral dopants were derivatives of *S*-1-phenylethylamine (**2**,**3**) and *S*-1-benzylethylamine (**4**–**7**) [12].

The chiral dopant **7** is non-mesomorphic and chiral dopants **2**–**6** are smectic; their mesomorphic characteristics are presented in the table.

The structural similarity between the non-chiral matrix and the chiral dopants and their miscibility in any proportion allowed us to study the phase diagrams over the entire concentration range.

3. Experimental

The identification of mesophase types was achieved using thermal polarizing optical microscopy, X-ray diffraction and helical pitch measurements. Textural analysis was realized using a Polam P-111 microscope. The samples were sandwiched between two glass plates which were previously treated with a surfactant and rubbed in one direction. The sample thickness was varied from 14 to 40 μm. The mounted material was confined in a specially constructed cell which had a $\pm 0{\cdot}5^\circ$ temperature control accuracy.

X-ray scattering experiments were performed on samples contained in 1 mm glass capillaries. Monochromatic CuK_α radiation (30 kV, 30 mA, focus size $0{\cdot}4 \times 8\ \text{mm}^2$, X-ray wavelength $\lambda_x = 1{\cdot}541$ Å) was used as the X-ray source in the range $2\theta = 0{\cdot}1$–5°. The instrumental resolution was $0{\cdot}02^\circ$ in the scan direction. The helical pitches of cholesteric and TGB phases were determined by the Grandjean–Cano method and from the peak wavelengths of selective transmittance bands which were measured using a Hitachi-330 spectrophotometer [9].

Temperatures of phase transitions for the non-chiral matrix and some mixtures were determined by differential scanning calorimetry using a Sateram DSC-111 calorimeter. The heating rates were $0{\cdot}5^\circ\text{C min}^{-1}$ and 2°C min^{-1}.

As a result of the measurements which were carried out the phase diagrams of the liquid crystalline systems studied were obtained (see figures 1–6). The temperatures of I–N*, N*–TGB, TGB–SmC* or TGB–SmA transitions are for cooling; the temperatures of the Cr–SmC* and Cr–SmA transitions relate to heating, as the mixtures undergo supercooling.

4. Results and discussion

Phase diagrams of all the systems studied have the following general features: the TGB phases lie between the N* and SmC* or SmA phases; blue phases are observed practically within the same concentration range as that for TGB phases; there is a critical point B in which the SmC*, TGB and SmA phases meet. At this point a division of the TGB region into two zones can be recognized, one which is intermediate between the N* and SmC* phases and the other which is intermediate between the N* and SmA phases (see figures 1–6).

Data obtained by X-ray diffraction enabled us to

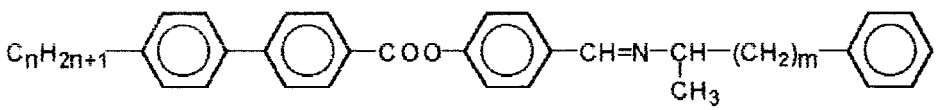

2 $m = 0$, $n = 9$; **3** $m = 0$, $n = 11$

4 $m = 1$, $n = 7$; **5** $m = 1$, $n = 9$; **6** $m = 1$, $n = 11$

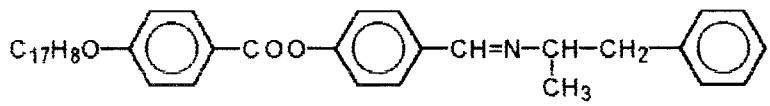

Table. Transition temperatures (T/°C), enthalpies (ΔH/kJ mol^{-1}), overall mesophase ranges (ΔT/°C) and twisting powers (β/μm^{-1} mol fr^{-1}) for the chiral dopants **2**–**7**.

		T (ΔH)[a]											
Dopant	n		Cr		SmC*		SmA		I	ΔT	$-\beta$[b]
2	9	heating	•	98·0 (28·0)	—		•	107·3 (4·2)	•	9·3	43·2 ± 2·2
	9	cooling	•		—	76·2 (23·2)	•	106·5 (4·1)	•	30·3	
3	11	heating	•	69·2 (33·7)	•	82·3 (<0·1)	•	101·6 (3·7)	•	32·4	40·5 ± 1·7
	11	cooling	•	<20	•	80·6 (<0·1)	•	99·5 (3·5)	•	>70·0	
4	7	heating	•	122·5 (41·9)	—		•	127·0 (2·0)	•	4·5	33·4 ± 1·1
	7	cooling	•		—	90·3 (31·9)	•	125·1 (2·0)	•	34·8	
5	9	heating	•	103·2 (37·7)	—		•	126·2 (3·4)	•	23·0	32·8 ± 1·0
	9	cooling	•		—	75·8 (27·7)	•	124·7 (3·3)	•	48·9	
6	11	heating	•	97·8 (35·9)	—		•	122·7 (4·2)	•	24·9	34·6 ± 2·2
	11	cooling	•	59·8 (18·7)	•	70·0 (3·1)	•	121·1 (4·2)	•	61·3	
7	8	heating	•	74·2 (50·4)	—		—		•	0	27·6 ± 0·8

[a] DSC data [12].
[b] Data for β in 4-pentyl-4′-cyanobiphenyl [12]. The values of β for compounds **2** and **5** in the ester 4-hexyloxyphenyl 4-octyloxybenzoate are, respectively, 17·3 ± 0·3 and 15·4 ± 2·3 μm^{-1} mol fr^{-1} at $T = T_i - 5°$; the values of β for the same compounds in the isomeric ester 4-octyloxyphenyl 4-hexyloxybenzoate are 17·1 ± 0·4 and 13·4 ± 0·3 [14], respectively.

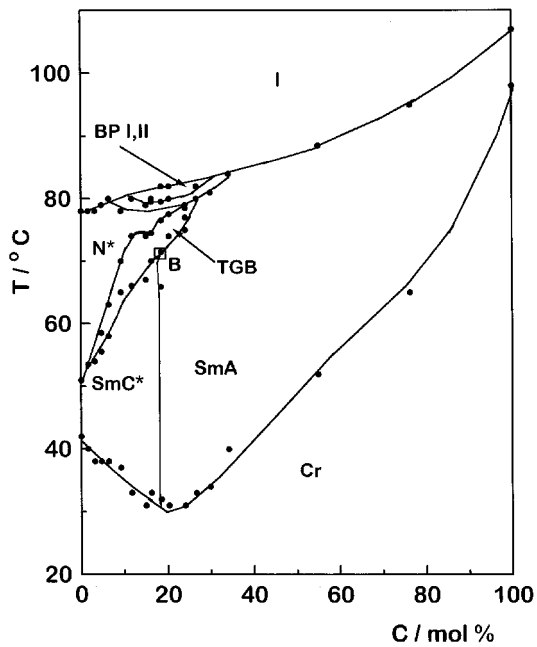

Figure 1. The phase diagram of the system **1**–**2**; c = mol % of **2** in **1**.

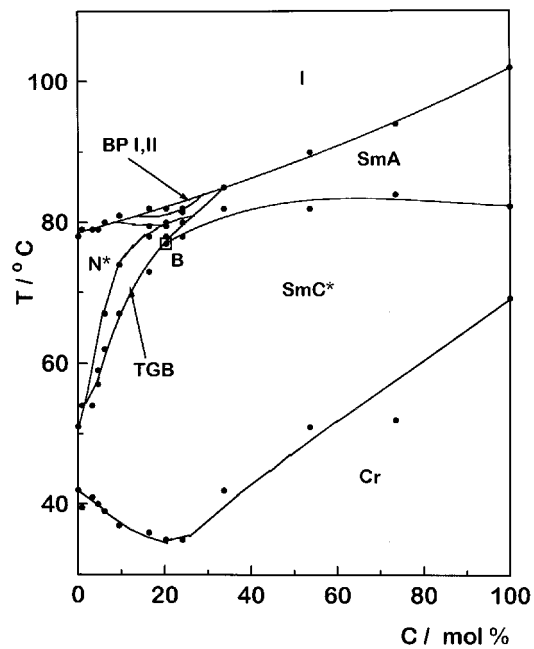

Figure 2. The phase diagram of the system **1**–**3**; c = mol % of **3** in **1**.

estimate the different structures of the TGB states corresponding to the two zones in the phase diagrams. Using the values of the layer spacing d measured by X-ray diffraction for the SmC* and TGB phases, and the molecular length of the non-chiral mesogens calculated in their most extended conformations (l = 31·0 Å), we obtained the tilt angle of the director relative to the smectic layer normal (θ_c). By such an approximate calculation, we consider that within a relatively small concentration range of chiral dopant (0–24 mol %) the smectic layers are statistically formed by a matrix of non-chiral molecules without regard for the chiral dopant.

The temperature dependences of θ_c for the systems **1**–**5** and **1**–**7** with different concentrations of chiral dopant are shown in figure 7. As is evident from the

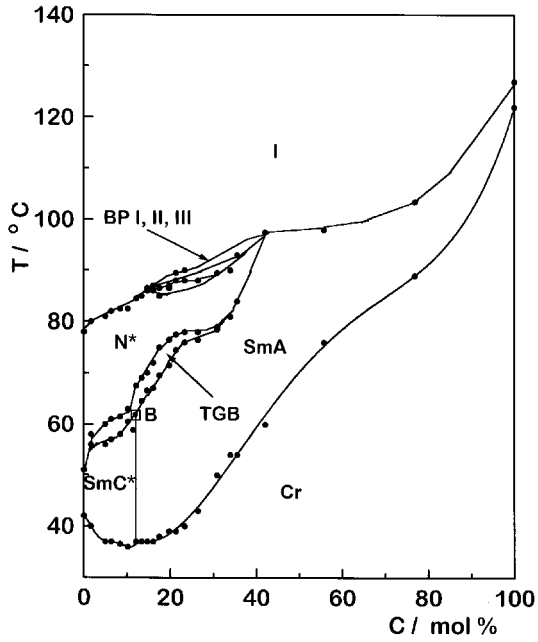

Figure 3. The phase diagram of the system **1**–**4**; c = mol % of **4** in **1**.

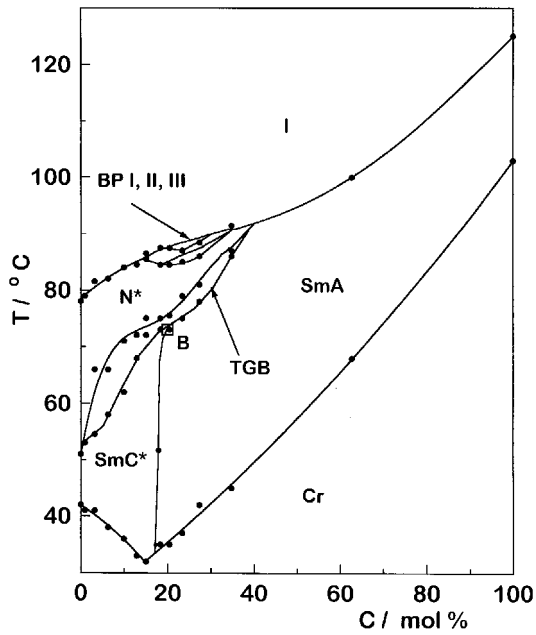

Figure 4. The phase diagram of the system **1**–**5**; c = mol % of **5** in **1**.

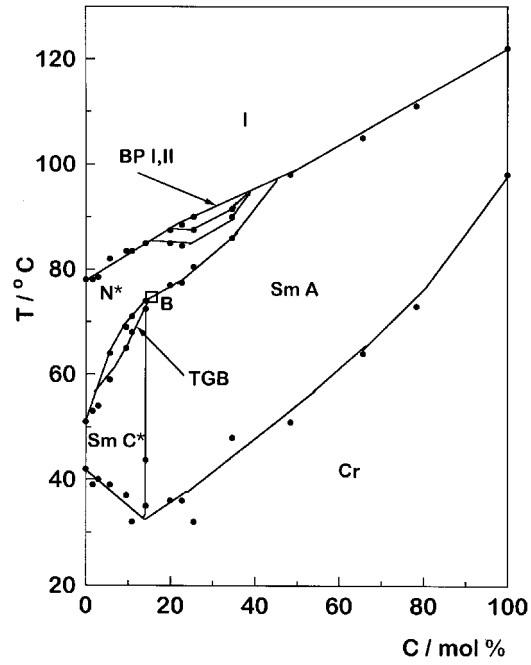

Figure 5. The phase diagram of the system **1**–**6**; c = mol % of **6** in **1**.

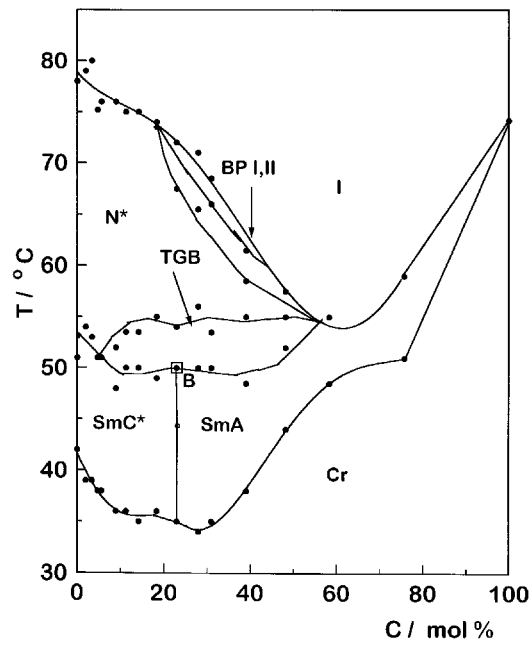

Figure 6. The phase diagram of the system **1**–**7**; c = mol % of **7** in **1**.

figure, the values of θ_c decrease with increasing temperature and chiral dopant concentration. As the chiral dopant concentration increases, the slope of $\theta_c(T)$ grows (compare curve 1 with 2, and curve 3 with 4 and 5). The θ_c have reasonably high values at small chiral dopant concentrations, when the wide TGB region is over the SmC* phase (curves 1, 3). These values decrease considerably as the chiral dopant concentration increases and the SmC*–SmA boundary is approached (curves 2, 5). For the **1**–**5** and **1**–**7** systems, the high values of θ_c are preserved at the SmC*–TGB phase transitions (curves 1, 4). This suggests that the TGB state over the SmC* phase has the TGB_C structure. In the case of the systems

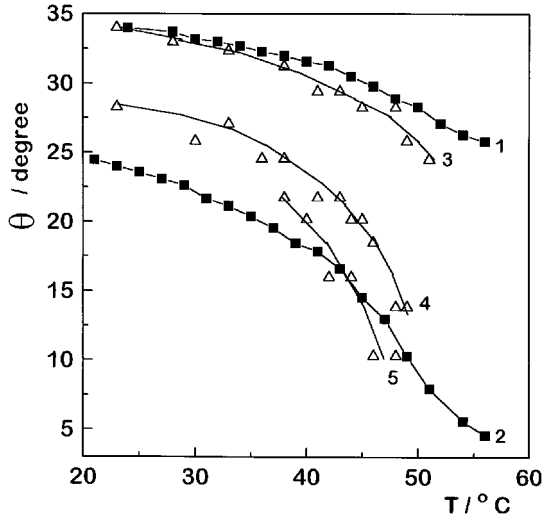

Figure 7. The temperature dependences of the tilt angles (θ) for the systems **1**–**5** (curves 1, 2) and **1**–**7** (curves 3–5): curve 1–3·15 mol % of the chiral dopant; curve 2–14·65 mol % of the chiral dopant; curve 3–5·62 mol % of the chiral dopant; curve 4–14·18 mol % of the chiral dopant; curve 5–22·94 mol % of the chiral dopant.

with high chiral dopant concentrations, the values of θ_c decay practically to zero at the SmA–TGB transitions (curves 2, 5). Therefore, the TGB states above the SmA phases may be considered as TGB_A phase, where the molecules are normal to the smectic layers.

The above conclusion about the different structures of the two TGB states is confirmed by textural studies. The appearance of the observed textures for the systems with the TGB phase on the SmC* side (for example, system **1**–**7** with 14·18 mol % of chiral dopant) is the following. On cooling from the isotropic liquid, a 'net' of regular disclinations appears in the plane cholesteric texture; then the cholesteric texture converts into a 'disclination net' texture at the N*–TGB phase transition and this is preserved over the TGB temperature range. On subsequent cooling, this texture transforms into the zig-zag folding texture of the SmC* phase. Other textural changes are observed for the system having the TGB phases on the SmA side. In the case of the 33·23 mol % system **1**–**7**, the plane cholesteric texture transforms into the 'platelet' texture of the TGB phase at the N*–TGB phase transition. The polygonal shaped domains of this texture have boundaries with steps typical of the SmA phase. The fan-shaped texture of the SmA phase appears on subsequent cooling. Similar textural changes have been recently reported in reference [10].

The division of the TGB region into two zones observed in all phase diagrams and the experimental evidence for the different structures of the mesophases corresponding to these zones is consistent with Renn's model version for TGB_A and TGB_C phases.

As shown in figure 7, the chiral dopants used lead to the tilt angle decreasing in the smectic C* layers. Due to this capacity of the chiral dopants, the induced SmA phase appears in the case of the system with the non-mesomorphic compound **7** (see figure 6). We presume that a θ_c decreasing with temperature and concentration increase is an important factor in relation to the occurrence of SmC*–TGB_C and SmA–TGB_A polymorphism.

Analysis of the phase diagrams reveals an appreciable effect of chiral dopant molecular structure on the TGB phase regions. Since TGB states are observed only for chiral liquid crystals, it was reasonable to consider an influence of the chiral dopant helical twisting power on the TGB phase regions. For that analysis we used data for the helical twisting power β of the chiral dopants in 4-pentyl-4′-cyanobiphenyl (5CB) (see the table) [12, 13]. It is evident from the data that the values of β for the chiral dopants **2** and **3** ($m=0$) are higher then the values of β for the chiral dopants **5**–**7** ($m=1$). An analogous tendency in the change of β is observed for the chiral dopants **2** and **5** in 4-*n*-hexyloxyphenyl 4-*n*-octyloxybenzoate and 4-*n*-octyloxyphenyl 4-*n*-hexyloxybenzoate (see footnote to table) [14]. On the basis of conformational analysis, this difference was explained by a capability of the *S*-1-benzylethylamine derivatives to adopt in the mesophase more anisometric, but less chiral conformations compared with the *S*-1-phenylethylamine derivatives [12, 13]. A chiral dopant's helical twisting power depends mainly on the extent of its π-conjugated molecular skeleton and this manifests itself in the lower value of β for the compound **7** as compared with compounds **4**–**6**. Moreover, it has been found [12, 13] that a chiral dopant's helical twisting power does not depend on the terminal alkyl chain length for the same extension of the π-conjugated molecular skeleton (see the table, compounds **2**, **3** and **4**–**6**).

The chiral dopant **7** with the lowest helical twisting power induces TGB phase formation up to 50 mol % (see figure 6). The TGB phase concentration region decreases with increase in the chiral dopant's helical twisting power. For the system **1**–**5**, the TGB phase region extends up to 40 mol % of chiral dopant **5** and for the system **1**–**2**, only to 30 mol % of dopant **2** (see figures 2, 4), so chiral dopant **5** has a lower helical twisting power than chiral dopant **2** at the same alkyl chain length ($n=9$).

However, it is obvious from the phase diagrams that the extent of the TGB phase region is determined not only by the helical twisting power of the chiral dopants, but also by the dopant's own smectic mesomorphism. As the alkyl chain length increases in the same series of smectogenic chiral dopants ($m=0$ or $m=1$), the SmA temperature range widens and smectic polymorphism appears (see the table). The TGB phase region decreases

with enhanced smectogenicity of the chiral dopant (compare figure 1 with 2 and figures 3 and 4 with 5). The TGB_A phase region is more sensitive to enhancement of the chiral dopant's smectogenicity; in particular this region disappears completely for system **1**–**6** (figure 5). Therefore, the greatest extension of the TGB phase concentration region for system **1**–**7** is caused not only by the lowest helical twisting power of chiral dopant **7**, but by its non-mesomorphic nature.

As follows from the phase diagrams, the maximum temperature range of the TGB_C phase (ΔT_{TGB_C}) is wider than that of the TGB_A phase (ΔT_{TGB_A}) for the systems with chiral dopants **2**–**6**; in the case of system **1**–**7**, the ΔT_{TGB_C} and ΔT_{TGB_A} are practically equal. The maximum temperature ranges of both the TGB_A and TGB_C phases change insignificantly for all systems studied (the values of ΔT_{TGB_C} are 5→9° and the values of ΔT_{TGB_A} are 1·5→6·5°). However, some tendency of the chiral dopant to influence the temperature range of the TGB_A phase is noted. For example, the values of ΔT_{TGB_A} decrease with the enhancement of the chiral dopant's smectogenicity from 3·5° for system **1**–**2** to 1·5° for system **1**–**3**, and from 5·5° for system **1**–**4** to 4° for system **1**–**5**, and the value of ΔT_{TGB_A} drops to zero for system **1**–**6**. The similar effect observed for the chiral dopant's influence on the temperature and concentration regions of the TGB phases is in agreement with Renn's model TGB phase diagram.

It follows from the above results that the TGB phase's concentration and temperature regions are determined by several macroscopic parameters of the liquid crystalline systems. In the case of induced chiral liquid crystalline systems, it is possible to observe separately how the helical cholesteric twist (P^{-1}) affects the TGB_C or TGB_A phase temperature ranges. The variation of the values of P can be realised by a ratio change of the optically active and racemic forms of the dopant at a constant total concentration. Measurements of the $\Delta T_{TGB}(P^{-1})$ were carried out for the system **1**–**5** at small (8·01 mol %) and high (23·5 mol %) total concentrations of the dopant **5**. The systems with these concentrations have TGB_C and TGB_A phases, respectively.

The experimental dependences of $\Delta T_{TGB}(P^{-1})$ were compared with Renn's theoretical relation:

$$\Delta T_{TGB} = B T_{NSm} (d/P)^{2/3} = A K_{22}^{2/3} T_{NSm} (d/P)^{2/3} \qquad (1)$$

where A is a constant, K_{22} is the twist elastic constant, T_{NSm} is the N–Sm transition temperature in the non-chiral liquid crystalline system, and d is the layer spacing. Under the above mentioned experimental conditions, the values of K_{22} and d are constant at the given total concentration of the dopant. This allows a linear approximation of the experimental dependences $\Delta T_{TGB}(P^{-1})$. In the case of the dopant at small concentration, it was assumed that the value d is determined by the molecular length of the non-chiral mesogens in their most extended conformations (l=31·0 Å). For the high concentration system, taking into consideration the effect of the longer molecules of the dopant (l=35·5 Å [9]), we used the value of d obtained by X-ray diffraction measurements (d=31·2 Å). The transition temperatures T_{NSm} for the non-chiral systems with the 8·01 and 23·5 mol % racemic dopant concentrations were 338 and 351 K, respectively.

The dependences of $\Delta T/T_{NSm}$ on $(d/P)^{2/3}$ are presented in figure 8. The linear character of these dependences suggests that Renn's relation (1) performs well (the correlation coefficient R is 0·949 for TGB_C and 0·971 for TGB_A). The different slopes a of the $\Delta T_{TGB}/T_{NSm}$ on $(d/P)^{2/3}$ indicate that ΔT_{TGB_C} is more sensitive to a change of the cholesteric twist than ΔT_{TGB_A} (a is 1·57 ± 0·6 for TGB_C and 0·56 ± 0·2 for TGB_A). Possibly, this experimental fact is explained by the different values of K_{22} in the cholesteric phase above the TGB_C and TGB_A phase, respectively.

5. Conclusion

For the liquid crystalline systems consisting of smectic non-chiral esters and structurally similar chiral dopants, the helical twisting power and the inherent smectogenicity of the chiral dopants influence considerably the overall concentration and temperature ranges of the TGB phases. However, the properties of these chiral dopants influence differently the two types of TGB regions (TGB_A and TGB_C). Whereas the concentration and temperature regions of the TGB_C phases are deter-

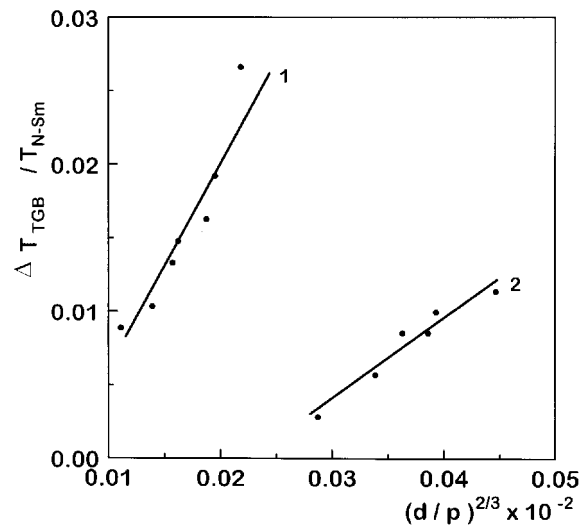

Figure 8. The dependences of $\Delta T_{TGB}/T_{NSm}$ on $(d/P)^{2/3}$ for the system **1**–**5**. Total concentration of the compound 5 (optically active and racemic forms) is 8·01 mol % (curve 1) and 23·5 mol % (curve 2).

mined mainly by the cholesteric helical twist, the TGB_A phase regions are sensitive to enhancement of chiral dopant smectogenicity. At the same time, mesomorphism for the chiral dopant is not necessary for the appearance of TGB states, if the disordering effect of the chiral dopant on the mesophase is insignificant.

The quantitative relation found experimentally between the temperature range of the TGB phases and the cholesteric helical twist correlates well with Renn's model relation.

This work was supported by the Ukraine Science Foundation for Investigations under grant No. 2.3/514.

References

[1] De Gennes, P. G., 1972, *Solid State Commun*., **10,** 753.
[2] Renn, S. R., and Lubensky, T. C., 1988, *Phys. Rev. A*, **38,** 2132.
[3] Renn, S. R., 1992, *Phys. Rev. A*, **45,** 953.
[4] Goodby, J. W., Waugh, M. A., Stein, S. M., Chin, E., Pindak, R., and Patel, J. S., 1989, *Nature*, **337,** 449.
[5] Ihn, K. J., Zasadzinski, J. A. N., Pindak, R., Slaney, A. J., and Goodby, J. W., 1992, *Science*, **258,** 275.
[6] Werth, M., Nguyen, H. T., Destrade, C., Isaert, N., 1994, *Liq. Cryst*., **17,** 863.
[7] Ribeiro, A. C., Dreyer, A., Oswald, L., Nicoud, J. F., Soldera, A., Guillon, D., and Galerne, Y., 1994, *J. Phys. II France*, **4,** 412.
[8] Dierking, I., Giebelmann, F., and Zugenmaier, P., 1994, *Liq. Cryst*., **17,** 17.
[9] Kramarenko, N. L., Semenkova, G. P., Kulishov, V. I., Tolochko, A. S., Kutulya, L. A., Vaschenko, V. V., and Handrimailova, T. V., 1992, *Kristallografiya*., **37,** 1266 (in Russian).
[10] Kramarenko, N. L., Semenkova, G. P., Kulishov, V. I., Tolochko, A. S., Kutulya, L. A., Vaschenko, V. V., and Handrimailova, T. V., 1994, *Liq. Cryst*., **17,** 351.
[11] Kramarenko, N. L., Kutulya, L. A., Kulishov, V. I., Tolochko, A. S., Semenkova, G. P., and Seminozhenko, V. P., 1994, *Zhurn. fiz. Khimii*, **68,** 1008 (in Russian).
[12] Kutulya, L. A., Semenkova, G. P., Kramarenko, N. L., Kulishov, V. I., Patsenker, L. D., Tolochko, A. S., and Batrachenko, L. A., 1994, *Funct. Mater*., **1,** 128.
[13] Kutulya, L. A., Semenkova, G. P., Yarmolenko, S. N., Fedoryako, A. P., Novikova, I. E., and Patsenker, L. D., 1993, *Kristallografiya*., **38,** 183 (in Russian).
[14] Semenkova, G. P., Kutulya, L. A., and Shkolnikova, N. I., *Kristallografiya*. (in the press).